

# EARLY ENTRY ANALYSIS OF CYGNUS NG-20

David Leiser<sup>(1)</sup>, Clemens Müller<sup>(1)</sup>, Martin Eberhart<sup>(1)</sup>, Stefan Löhle<sup>(1)</sup>, Gerard Armstrong<sup>(2)</sup>, Byrenn Birch<sup>(2)</sup>, Andrew Lock<sup>(2)</sup>, Ranjith Ravichandran<sup>(2)</sup>, Fabian Zander<sup>(2)</sup>, Savio Poovathingal<sup>(3)</sup>, and Alexandre Martin<sup>(3)</sup>

<sup>(1)</sup>High Enthalpy Flow Diagnostics Group (HEFDiG), Institute of Space Systems, University of Stuttgart, 70569, Germany

<sup>(2)</sup>University of Southern Queensland, Toowoomba, Queensland 4350, Australia

<sup>(3)</sup>University of Kentucky, Lexington, Kentucky, 40506, USA

## ABSTRACT

On the 13th of July 2024, the ISS resupply capsule CYGNUS NG-20 entered the Earth's atmosphere above the South Pacific for a controlled destructive re-entry, marking the end of the mission. The capsule was equipped with 5 re-entry experiments (KRUPS - Kentucky Re-Entry Universal Payload System) from the University of Kentucky. The re-entry of CYGNUS was observed from an aircraft equipped with four instrument platforms capturing imaging, spectroscopic, and polarization data which were time-synchronized using a GPS signal.

While the initial goal of the mission was to observe the KRUPS capsules after their release from the spacecraft, a delay in in-space operation shifted the trajectory down-range complicating this objective. HEFDiG deployed a new spectroscopic camera system using a transmission grating. This camera is able to detect spectra between 400 nm and 700 nm with a theoretical resolution of 0.4 nm per pixel. Finally, the altitude region of 93 km to 70 km was successfully observed giving insight into the early entry phase before the main break-up and significant fragmentation occurs. During this phase only broadband radiation was detected indicating black-body radiation from aerothermal heating of the spacecraft. Finally the break-up was observed in one frame corresponding to an altitude of 73 km.

Keywords: CYGNUS NG-20; Re-Entry; Airborne Observation.

## 1. INTRODUCTION

Over the past decades, a multitude of missions have been flown to observe the re-entry of a variety of bodies into Earth's atmosphere. The observed bodies range from sample return capsules [1, 2, 3], space debris such as WT1190F [4] and the Cluster satellite *Salsa* [5] to the ISS resupply vehicles ATV-1 [6, 7, 8] and CYGNUS OA-6 [6, 9].

These missions have greatly improved the knowledge of different processes during re-entry especially break-up and demise of spacecraft returning from low earth orbit.



Figure 1. CYGNUS NG-20 during unberthing from the International Space station 12th of July 2024 [10].

The Kentucky Re-entry Universal Payload System (KRUPS) was developed to test the performance of different Thermal Protection System (TPS) materials at a fraction of the cost to full-scale re-entry experiments [11, 12]. Sounding rocket experiments preceded the Kentucky Re-Entry Probe Experiment (KREPE), which occurred during the re-entry of the ISS resupply vehicle CYGNUS NG-16 in 2021 and featured three capsules.

A preliminary analysis of this data [12] proves the capabilities of this system while open questions regarding trajectory and flight path remain. Therefore during the subsequent KREPE-2 mission, an airborne observation mission was planned to correlate the data from the capsules with observation data. The KREPE-2 mission consisted of five KRUPS capsules [13], which were launched onboard the CYGNUS NG-20 resupply vehicle. Operations remained identical to the KREPE-1 mission where the capsules were activated shortly before the CYGNUS vehicle was unberthed from the space station. Release of the spacecraft took place on July 12th 2024 11:01 UTC and the spacecraft successfully deorbited 13th of July at 16:00 UTC.

## 2. MISSION

The team at the University of Southern Queensland (UniSQ) organized the aircraft used for observation, provided by GCH Aviation. The Bombardier Challenger 604 business jet is based in Christchurch New Zealand, where integration of the instruments and testing took place. The aircraft featured standard windows made of acrylic with no alterations, meaning that transmission below 400 nm is significantly, making observation in the UV extremely challenging.



Figure 2. Bombardier Challenger 604 aircraft used for the observation mission.

Three flights were planned to position the aircraft in the target area and orientation. The first flight was used to relocate personnel and equipment to the staging area, in Avarua, Rarotonga, Cook Islands. From here the mission was flown followed by another relocation flight to Christchurch.

Due to a delayed release of the spacecraft from the international space station all orbit adjustment maneuvers, including the re-entry burn were delayed by around 4 minutes. This shifted the re-entry trajectory around 1900 km to the southeast, shown in Fig. 3. Due to this, it was not possible to position the aircraft in the relative position previously planned to observe the release and entry of the KRUPS capsules, rather the observation targeted the early entry phase. This was due to the maximum range of the aircraft, coupled with the flight restricted areas due to the re-entry. Signal acquisition was calculated to occur at 16:03:00 corresponding to an altitude of 90 km, with signal loss at 16:07:30, 70 km.

The aircraft positioning and tracking is described separately in detail [14]. The calculated position of the spacecraft during re-entry relative to the aircraft normal plane is shown in Fig. 4. The aircraft flies a turn to maximize the time during which the re-entry is visible

## 3. EXPERIMENTAL ARRANGEMENT

In total 6 stations distributed over 6 windows were used to observe the re-entry of the CYGNUS NG-20 spacecraft featuring 16 instruments in total. Four platforms tracked the entry manually. This paper focuses on the station operated by the High Enthalpy Flow Diagnostics Group (HEFDiG) which was equipped with two instruments.

Image acquisition and tracking of the spacecraft was realized using an Alvim 1800 U-508m camera during the observation time and movement of the aircraft. Settings and recording were controlled using custom software. Both the camera and the software were provided by UniSQ. The nominal camera parameters are shown in table 1.

Parameter	Value
Image Height	1028 px
Image Width	1232 px
Binning	2x2
Gain	35
Bit Depth	8 bit mono
Exposure Time	30 ms

Table 1. Nominal Parameters used for the tracking camera

Aiming for a fast acquisition, a 2x2 binning was applied and the bit depth was set to 8 bit which allows to increase the frame rate as well as increase the signal-to-noise ratio.

Aligned to the tracking camera is a Nikon Z8 camera with a 300 mm lens for spectrally resolved data acquisition. Unlike most commercial lenses that feature a filter holder before the entrance aperture, this lens features a 52 mm filter holder integrated into the lens body, just before the mounting point. This feature was used, by 3D-printing a holder for a 50 mm x 59 mm optical filter. Instead of a filter, an optical transmission grating with 300 lines per mm (*Thorlabs GT50-03*) was installed. This separates the incoming light into its spectral components which can be detected on the image sensor. The arrangement as well as the filter and sensor positions are sketched in Fig. 6.

The angular field of view (*AFOV*) of the camera system can be calculated using:

$$AFOV = 2 \cdot \arctan\left(\frac{H}{2f}\right) \quad (1)$$

with the image sensor size  $H$  and the focal length  $f$ , both in millimeters.

The deflection of the grating can be calculated using

$$\sin\theta = \frac{m\lambda}{d} \quad (2)$$

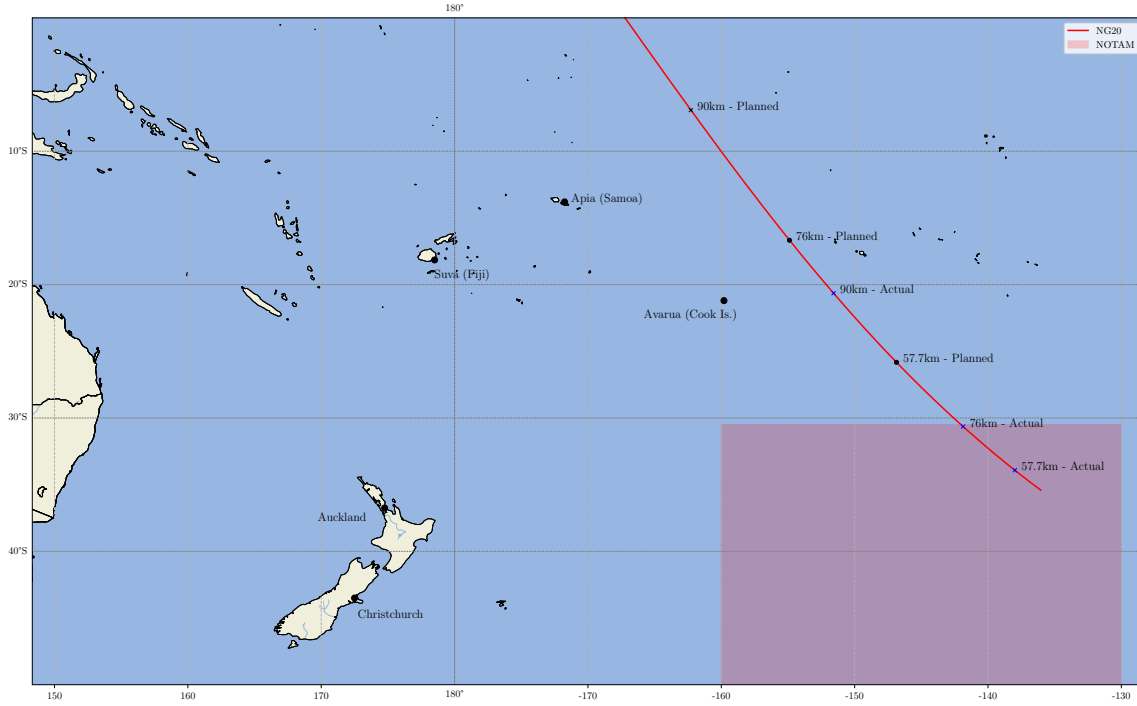


Figure 3. Ground track of the spacecraft with the shifted trajectory during the observation mission.

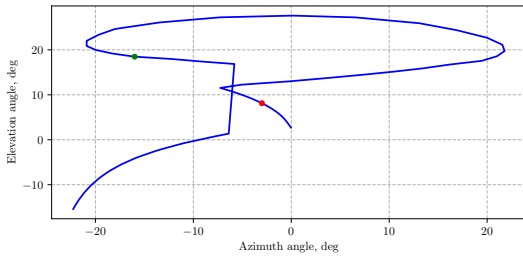


Figure 4. Azimuth and elevation of the calculated spacecraft trajectory.

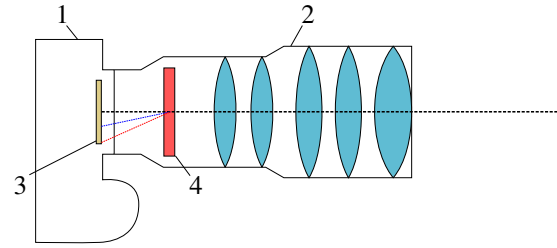


Figure 6. Diagram of the optical system to record spectral data using the Nikon Z8 system. 1 - Camera body; 2 - Lens; 3 - Camera sensor; 4 - Grating



Figure 5. Hardware used for the station operated by HEFDiG.

Parameter	
Sensor Size	35.9 mm x 23.9 mm
Focal Length	300 mm
Exposure Time	1/30 s
ISO	25600
Framerate	30 fps
AFOV	6.84° x 4.56°

Table 2. Camera Parameters

The resulting position on the sensor is

$$\tan\theta = \frac{y}{l_{\text{tot}}}, \quad (3)$$

where  $l_{\text{tot}}$  is the total distance between the grating and the sensor, in the present case 90 mm. The deflection, from the 0th order, of blue light (400 nm) can be calculated to 11 mm while the deflection of red light (700 nm) can be

calculated to 19 mm, in the sensor plane. This means that 30 % of the sensor height is needed to resolve the entire visible spectrum. While not necessary in all frames, it is very helpful for the data processing to also have the 0th order in the frame, i.e. light passing the grating without being spectrally shifted. Hereby, around 80 % of the frame are needed to resolve both the 0th order as well as red light from the first order. This leaves a margin of 0.9 degrees in the field of view to keep the target in frame, making accurate tracking challenging during the movement of the aircraft.

From the total pixel count as well as the diffraction, the theoretical spectral resolution results to 0.4 nm/px. However, to differentiate two close spectral lines one must apply the Rayleigh criterion further decreasing the usable resolution. For this analysis the point-spread-function for the spectral system was not determined, previous analyses on similar cameras exhibited a 6 px radius [15]. Applying this leads to a usable resolution of 2.4 nm.

### 3.1. Calibration

Wavelength and intensity calibration was performed on ground using known sources. The spectral calibration was performed using a mercury vapor lamp with the three most prominent lines used for calibration at 435.8, 546.0 nm, and 579.0 nm.

The distance from these lines to the zero-order light was determined in pixels. For small angles eqs 2 and 3 may be simplified whereby the deflection is linearly proportional to the wavelength,  $\lambda \propto y$ .

Recording the integrating sphere calibration source with a known irradiance allows for the intensity calibration using known methods [16]. This also highlights the wavelength range that is able to be recorded, from 400 nm to 700 nm which is typical for consumer cameras [17]. Two calibration methods were applied, one where the image is converted to grayscale and then calibrated, while the second method separates the image into each color channel, which is calibrated separately.

Separate calibration allows for an analysis of features that are at the edge of two channels, which may be image-processing artifacts rather than spectral features. Furthermore, noise in the blue wavelength range was stronger in the grayscale, compared to separate calibration due to color grading in the conversion process. This together with the low intensity of the calibration lamp in the blue region increased signal noise. A future step is also possible where the calibration procedure is modified, adapting the exposure time to maximize the intensity in each color channel in separate calibrations.

## 4. ANALYSIS

The signal was initially captured in the tracking camera, at 16:02:40 UTC. The light signature appeared over the horizon. The signal was simultaneously acquired in the Nikon camera; however, only the zeroth order was discernible from the background.

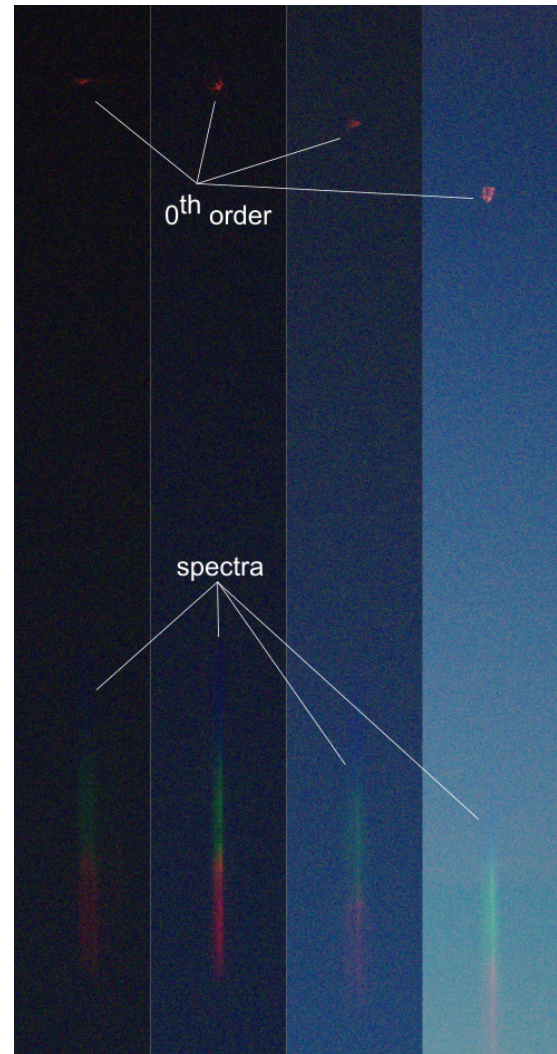


Figure 7. Cropped camera images of CYGNUS at 16:04:15 (left), 16:04:59 (middle-left), 16:05:34 (middle-right), and 16:06:52 (right).

The signal of the spectra was strong enough to discern it from the noise from 16:04:15 UTC onward. The recorded spectral data mainly shows a broad-band signature, indicating that black-body radiation from the heating spacecraft is detected. No distinct spectral features are discernible. A spectrum recorded shortly afterward detection is shown in Fig. 8. The highest signal-to-noise ratio was recorded at 16:04:59 UTC, shown in Fig. 9, which corresponds to the closest approach of the plane to the spacecraft at 16:05:03 at a distance of 281 km. Afterwards the signal intensity decreased with the increasing separation, as well as the changing viewing angle.

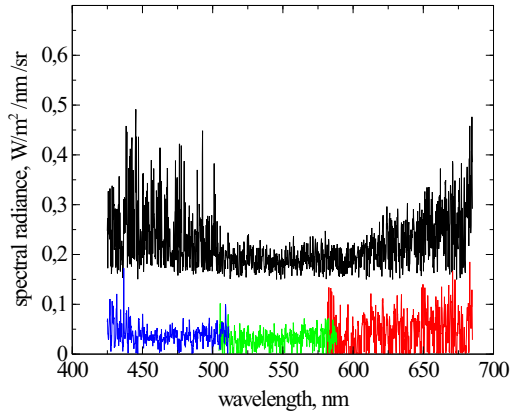


Figure 8. Calibrated spectrum at 16:04:29 showing the color channels as well as the grayscale spectra. Grayscale is offset by 0.15 for better visibility.

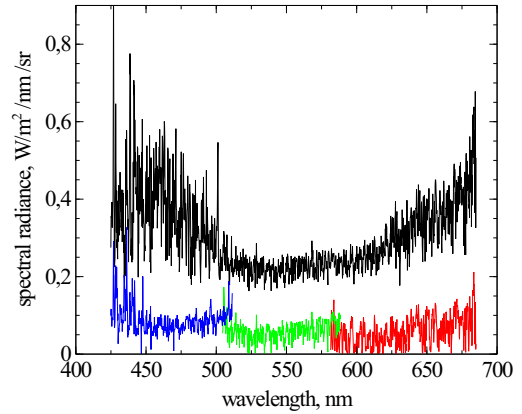


Figure 10. Calibrated spectrum at 16:05:34 showing the color channels as well as the grayscale spectra. Grayscale is offset by 0.15 for better visibility.

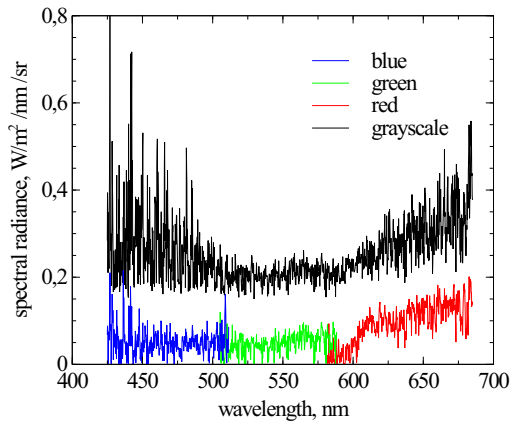


Figure 9. Calibrated spectrum at 16:04:59 UTC showing the color channels as well as the grayscale spectra. Grayscale is offset by 0.15 for better visibility.

During the observation, the relative motion of the aircraft and the Cygnus moved the spacecraft towards the east, where the sun was dawning. This meant an increased background, further complicating both tracking and signal acquisition. Towards the end of the observation, at 16:06:52 UTC, a bright flash appears for one frame in the tracking camera, shown in Fig. 11. This flash was also captured in the spectral camera, shown in Fig. 7. This is presumed to be the main break-up of the spacecraft, which corresponds to an altitude of 76 km, a typical break-up altitude for large spacecraft. The recorded broadband spectrum further highlights that the spectra are black-body radiation rather than reflections of the sun, since the event would not increase the reflectivity. At this time the distance between the aircraft and the spacecraft was 842 km.

Finally the signal was lost, at 16:06:54 UTC in the spec-

tral camera, at which point only the zeroth order was visible and 16:07:08 UTC in the tracking camera. In total, CYGNUS NG-20 was visible for 255 seconds of the re-entry covering the altitude range of 93 to 73. Spectra were discernible from background and noise for 65 seconds, in the altitude range of 87 km to 76 km.

As an estimation a Planck curve was fit to the spectra, an example frame of this is shown in Fig. 12. The temperature evaluated from this fit was fairly constant throughout the observation at 1300 K. As the temperature is expected to rise during this time, this value must be seen with caution.

## 5. CONCLUSION

A novel spectral camera system was used to observe the re-entry of the Cygnus NG-20 ISS resupply vehicle. This system comprises a Nikon Z8 camera with a transmission grating in the optical path for high-resolution, high-framerate spectroscopy. An Allied Vision Alvium U-508m camera is used for tracking and pointing. Cygnus NG-20 entered the Earth's atmosphere on July 13th, 2024, 4 minutes delayed to the scheduled time. This delay shifted the observed trajectory downrange meaning that the early entry phase was observed instead of the planned main break-up and fragmentation. Cygnus was visible for 255 seconds.

Recorded spectra showed black-body radiation mainly from aerothermal heating of the spacecraft. No spectral features were discernible during this phase. This corresponds to the re-entry of other large spacecraft, where most spectral features were visible shortly before or after the main break-up event [6].

The observation showed that the camera system is a versatile system, very compact and insensitive to airborne

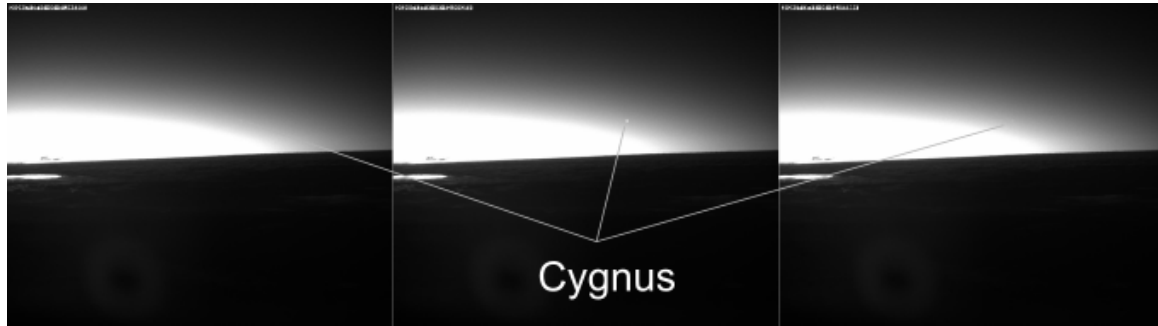


Figure 11. Tracking camera images at 16:06:52 showing a bright flash.

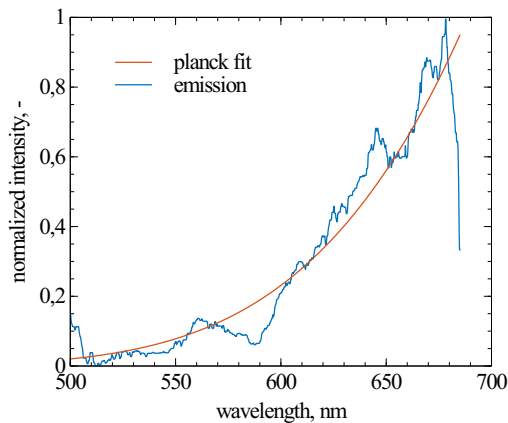


Figure 12. Smoothed spectrum and Planck fit ( $T = 1300\text{ K}$ ) of the signal recorded at 16:04:59.

observation vibrations. The instrument in its current state requires further investigation of the optical throughput. Therefore, a full analysis of the optical path including the grating at its new position is planned. Coupled with a point spread function analysis, this will allow the spectral resolution to be analyzed in detail. A re-analysis of the calibration routine, specifically multi-channel calibration, will allow for a reduction in the noise as well as reducing the artifacts at the transition between different color filter ranges. A further rather simple improvement might be to remove the color filter, so to use the camera as a monochrome system.

## ACKNOWLEDGMENTS

Funding for this project was provided by NASA Kentucky Space Grant Award. Martin and Poovathingal were supported by NASA ISS EPSCoR award KY-80NSSC21M0228, NASA Entry Systems Modeling Project, and the University of Kentucky. The authors would like to thank the team at GCH Aviation for their immeasurable support, as well as the mechanical workshop at IRS for their support in modifying the hardware.

Special thanks goes to the entire HEFDiG team for their support and discussions.

## REFERENCES

1. P. Jenniskens, P. Wercinski, J. Olejniczak, G. A. Raiche, D. A. Kontinos, G. A. Allen, P. N. Desai, D. Revelle, J. Hatton, R. L. Baker, R. W. Russell, M. Taylor, and F. Rietmeijer. Preparing for the hyperseed mac: An observing campaign to monitor the entry of the genesis sample return capsule. *Earth, Moon, and Planets*, (95), 2004. doi: 10.1007/s11038-005-9021-2.
2. Fabian Zander, David R. Buttsworth, Byrenn Birch, and Allan Payne. Trajectory analysis of the hayabusa2 capsule from a single airborne observation. *Journal of Spacecraft and Rockets*, 61 (1):173–180, 2024. ISSN 0022-4650. doi: 10.2514/1.A35719.
3. R. A. Williams, E. M. Queen, Soumyo Dutta, and C. D. Karlsgaards. Osiris-rex entry, descent, and landing performance. In *Scitech 2025 Forum*, Reston, Virginia, 2025. AIAA American Institute of Aeronautics and Astronautics. doi: 10.2514/6.2025-2424.
4. P. Jenniskens, J. Albers, M. Koop, M. Odeh, K. Al-Noimy, K. Al-Remeithi, K. Al-Hasmi, R. F. Dantowitz, F. Gasdia, S. Loehle, F. Zander, T. Hermann, D. Farnocchia, S. R. Chesley, P. W. Chodas, R. S. Park, J. D. Giorgini, W. J. Gray, D. K. Robertson, and T. Lips. Airborne observations of an asteroid entry for high fidelity modeling: Space debris object wt1190f. In *54th AIAA Aerospace Sciences Meeting*, AIAA SciTech Forum, Reston, VA, USA, 2016. AIAA American Institute of Aeronautics and Astronautics. doi: 10.2514/6.2016-0999.
5. C. Mueller, D. Leiser, M. Eberhart, S. Fasoulas, S. Loehle, F. Zander, B. Birch, R. Ravichandran, G. Armstrong, J. Toth, T. Paulech, P. K arr ang, T. Lips, J. Silha, M. Zigo, B. Jilete, B. B. Virgili, and S. Lemmens. First results from the salsa airborne re-entry observation mission campaign. In *9th Space Debris Conference*. 2025.

6. S. Loehle, F. Zander, S. Lemmens, and H. Krag. Airborne observations of re-entry break-up: Results and prospects. In *7th European Conference on Space Debris*, Darmstadt, Germany, 2017.
7. S. Loehle and R. Wernitz. Slit instrument results: High resolution spectroscopy of the Jules Verne re-entry. In *European Air and Space Conference*, Manchester, UK, 2009.
8. J. B. Snively, M. J. Taylor, and P. Jenniskens. Airborne imaging and NIR spectroscopy of the ESA ATV spacecraft re-entry: Instrument design and preliminary data description. *International Journal of Remote Sensing*, 32(11):3019–3027, 2011. doi: 10.1080/01431161.2010.541516.
9. S. Loehle, M. Eberhart, F. Zander, A. Meindl, R. Rudawska, D. Koschny, J. Zender, R. Dantowitz, and P. Jenniskens. Extension of the plasma radiation database for the analysis of meteor spectra. *Meteoritics and Planetary Science*, 2021. ISSN 1945-5100. doi: 10.1111/maps.13622.
10. NASA Johnson Space Center. Cygnus NG-20: ISS071e329982.
11. John D. Schmidt, James T. Nichols, Matthew P. Ruffner, Ryan D. Nolin, William T. Smith, and Alexandre Martin. Kentucky re-entry universal payload system (krups): Design and testing for hypersonic re-entry flight. In *AIAA SCITECH 2022 Forum*, Reston, Virginia, 2022. American Institute of Aeronautics and Astronautics. ISBN 978-1-62410-631-6. doi: 10.2514/6.2022-1576.
12. John D. Schmidt, Matthew P. Ruffner, James T. Nichols, Isaac S. Rowe, Ryan D. Nolin, Kirsten F. Ford, William T. Smith, and Alexandre Martin. Kentucky re-entry universal payload system (krups): Overview of hypersonic re-entry flight. In *SciTech 2023 Forum*, Reston, VA, USA, 2023. AIAA American Institute of Aeronautics and Astronautics. ISBN 978-1-62410-699-6. doi: 10.2514/6.2023-0206.
13. Matthew P. Ruffner, Kirsten F. Ford, Logan M. Craig, Bruno D. Tacchi, John D. Schmidt, Savio J. Poovathingal, William T. Smith, and Alexandre Martin. Overview of the hypersonic test flight Krepe-2. In *AIAA Aviation Forum*, Reston, Virginia, 2024. AIAA American Institute of Aeronautics and Astronautics. ISBN 978-1-62410-716-0. doi: 10.2514/6.2024-3561.
14. F. Zander and et. al. Airborne observation of the Cygnus NG-20 re-entry. In *Interplanetary Probe Workshop 2025*.
15. F. Grigat, S. Loehle, F. Zander, and S. Fasoulas. Spallation on carbon ablators. *AIAA Journal*, 60(7):3936–3949, 2022. ISSN 0001-1452. doi: 10.2514/1.J061276.
16. James M. Palmer and Barbara Geri Grant. *The art of radiometry*, volume 184 of *SPIE PM*. SPIE Press, Bellingham, Wash., 2010. ISBN 978-0-8194-7245-8.
17. K. Martišek and H. Druckmüllerová. A numerical method for the visualization of the Fe XIV emission in the solar corona using broadband filters. *The Astrophysical Journal Supplement Series*, 197(2): 23, 2011. ISSN 0067-0049. doi: 10.1088/0067-0049/197/2/23.